

# Image Blind Denoising Using Dual Convolutional Neural Network with Skip Connection

Wencong Wu<sup>a</sup>, Shicheng Liao<sup>a</sup>, Guannan Lv<sup>a</sup>, Peng Liang<sup>a</sup>, Yungang Zhang<sup>a,\*</sup>

<sup>a</sup>*School of Information Science and Technology, Yunnan Normal University, Kunming 650500, Yunnan Province, China*

---

## Abstract

In recent years, deep convolutional neural networks have shown fascinating performance in the field of image denoising. However, deeper network architectures are often accompanied with large numbers of model parameters, leading to high training cost and long inference time, which limits their application in practical denoising tasks. In this paper, we propose a novel dual convolutional blind denoising network with skip connection (DCBDNet), which is able to achieve a desirable balance between the denoising effect and network complexity. The proposed DCBDNet consists of a noise estimation network and a dual convolutional neural network (CNN). The noise estimation network is used to estimate the noise level map, which improves the flexibility of the proposed model. The dual CNN contains two branches: a u-shaped sub-network is designed for the upper branch, and the lower branch is composed of the dilated convolution layers. Skip connections between layers are utilized in both the upper and lower branches. The proposed DCBDNet was evaluated on several synthetic and real-world image denoising benchmark datasets. Experimental results have demonstrated that the proposed DCBDNet can effectively remove gaussian noise in a wide range of levels, spatially variant noise and real noise. With a simple model structure, our proposed DCBDNet still can obtain competitive denoising performance compared to the state-of-the-art image denoising models containing complex architectures. Namely, a favorable trade-off between denoising performance and model complexity is achieved. Codes are available at <https://github.com/WenCongWu/DCBDNet>.

*Keywords:* Image Denoising, Dual CNN, Skip Connection, Dilated Convolution, Noise Estimation Network

---

## 1. Introduction

In the process of image acquisition and transmission, noise is hardly to be avoided, which seriously affects the visual quality of images, therefore noise removal is an extremely important step for many image processing tasks [1]. All denoising methods aim to obtain the clean image  $x$  from its noisy observation  $y$  by eliminating the noise  $n$ , namely  $x = y - n$ . Over the decades, many denoising methods have been proposed. For instance, the non-local means (NLM) [2] uses the average of all pixels in an image to achieve noise filtering. In GNLM [3], the grey theory [4] is integrated into the NLM to further improve its denoising performance. Targeted image denoising (TID) [5] improves denoising performance by using a dataset that contains similar image patches. Block-matching and 3-dimensional filtering (BM3D) [6] enhances the sparse representation by collaborative alteration for image denoising. The learned simultaneous sparse coding (LSSC) [7] combines the non-local means and sparse coding approaches to realize noise removal. Other denoising methods based on non-local self-similarity (NSS) [8, 9], sparse learning [10, 11, 12], gradient learning [13, 14, 15, 16], Markov random field (MRF) [17, 18, 19, 20], total-variation (TV) [21, 22], and weighted nuclear norm minimization (WNNM) [23, 24] were also proposed.

Although the above-mentioned traditional denoising methods have achieved favorable denoising performance, most of these approaches have two shortcomings: (1) the complex optimization algorithms of these methods lead to massive running time consumption, and (2) many models require a considerable number of manual setting parameters,

---

\*Corresponding author

*Email address:* [yungang.zhang@ynnu.edu.cn](mailto:yungang.zhang@ynnu.edu.cn) (Yungang Zhang)

which increases the uncertainty of denoising results. There are some denoising methods based on image priors such as the fields of experts [18], cascade of shrinkage fields (CSF) model [25], or the trainable nonlinear reaction diffusion (TNRD) [26], they do not need time-consuming optimization procedures, or less manually set parameters are required during model training, however the performances of these methods are limited by the specific forms of image priors. Inspired by the CSF and TNRD, Zhang et al. [27] proposed a successful denoising convolutional neural network (DnCNN). However, the DnCNN performs well only in a limited range of noise levels. Since the advent of DnCNN, deep neural networks (DNN) based models have become the most popular denoising methods [28, 29]. However, the early DNN based denoising models like DnCNN need to train a specific model for a specific noise level, the limited flexibility of these models makes them hard to be utilized in real denoising scenes.

To make the DNN based denoising models more flexible, many techniques have been developed. Some researchers try to use a tunable noise level map as the network input [30, 31], therefore it is capable of handling a wide range of noise levels including spatially variant and invariant noise. However, the noise level map has to be manually pre-defined. To realize blind denoising, many models try to incorporate a noise estimation sub-network to obtain noise distribution in an image, such as the convolutional blind denoising network (CBDNet) [32], the blind universal image fusion denoiser (BUIFD) [33], and the variational denoising network (VDN) [34], promising denoising performances have been obtained.

Although increasing the depth of the neural networks may improve their learning ability, the problem of huge network parameters and high computational costs will also be brought, and it has been verified that the accuracy of the network will decline when the network depth is increased constantly, therefore many researchers have proposed to expand the width of the networks instead of the depth. Especially, in [35, 36, 37], the dual CNNs are designed for image denoising, illustrating that the competitive denoising performance can also be obtained by increasing the width of the deep neural network models.

Recently, many research works have revealed that the skip connection [38, 39], dilated convolution [40], and the U-Net [41] can be helpful for deep image denoising models. The dilated convolution and the U-Net can enlarge the receptive fields of convolution layers, and skip connection has the ability to accelerate network training, also they can provide better feature preservation during feature transposing. Some recently proposed denoising models such as IRCNN [42], DSNet [43], BRDNet [36], DRUNet [31], RDUNet [44], and the DDUNet [45] have achieved remarkable denoising performances by using these techniques.

Inspired by the success of the above-mentioned techniques in image denoising, in this paper, we propose a novel dual convolutional blind denoising network with skip connection (DCBDNet) to achieve effective denoising performance. The proposed DCBDNet model contains a noise estimation network and a dual convolutional neural network (CNN) with two sub-networks. In the proposed dual convolutional network, one sub-network is a u-shaped convolutional network, where the downsampling and upsampling are used. Another sub-network contains dilated convolutional layers to enlarge the receptive field of the convolution layers. Skip connections are employed in both sub-networks to fuse the features from different convolution layers. The features from the two sub-networks are then concatenated to produce the denoised image. The proposed DCBDNet owns the following favorable characteristics:

- (1) A noise estimation network with a large receptive field is designed, which can extract more useful information and estimate the noise level map accurately.
- (2) The dual CNN of the proposed DCBDNet utilizes downsampling operations and dilated convolutions to enlarge the receptive field. Moreover, skip connections are utilized to preserve more image details for denoising.
- (3) Experimental results verify that our proposed DCBDNet achieves more robust and efficient denoising performance than similar networks on both synthetic and real noisy images.

The remainder of this paper is organized as follows. Section 2 gives a brief introduction of the related image denoising techniques. Section 3 introduces our proposed model. Section 4 presents our experimental results. The paper is concluded by Section 5.

## 2. Related work

The dual sub-network structure is one of the methods that are used to expand the width of the network, where generally two different sub-networks are designed to achieve complementary feature learning. In [35], a DualCNN contains two sub-networks was proposed for low-level vision tasks, where the shallow branch is used for obtaining

the whole structure of an image, and another deeper branch is designed for capturing image details. Tian et al. [37] designed a dual denoising network (DudeNet), which can extract global and local features to enhance the network performance. A batch-normalization denoising network (BRDNet) was proposed in [36], which includes an upper and a lower sub-networks to increase the network width.

It is worth noting that the BRDNet [36] has a large difference in the sizes of the receptive fields in its upper and lower sub-networks, which may degrade its learning ability and denoising performance. In addition, the dilated rate of the dilated convolutions in BRDNet is fixed, which may lead to the loss of image details, generating the gridding phenomenon. The BRDNet with two 17-layer sub-networks has a deeper network structure and more network parameters. Moreover, in BRDNet, one network is trained for only one specific noise level, which leads to its inflexibility and impracticality. In this paper, we also develop a dual CNN structure, however we aim to design a more flexible denoising network to realize blind denoising. Different from the BRDNet, our dual CNN contains fewer layers. The downsampling and upsampling are used in our upper sub-network, and the hybrid dilated convolutions are utilized in the lower sub-network, which can augment the receptive field, and the sizes of the receptive fields of the two branches can keep close. More importantly, in our model, a noise estimation network is developed for obtaining a noise level map, which makes our model fully blind.

To address the problem of model flexibility, Zhang et al. [30] proposed a fast and flexible denoising convolutional neural network (FFDNet), and a tunable or non-uniform noise level map helps FFDNet can handle a wide range of noise levels including spatially variant and invariant noise, the DRUNet [31] also takes this type of noise level map as its input. DRUNet achieves the state-of-the-art denoising performance, however it has a large number of network parameters and a complex network structure. Moreover, since the noise distributions in a real noisy image are unknown, the manually defined noise level map used in the FFDNet and the DRUNet makes them hard to be applied in real denoising scenes.

In order to make a denoising model fully blind, many different techniques have been developed. In DeamNet [46], a dual element-wise attention mechanism (DEAM) module, and a new adaptive consistency prior (ACP) are introduced for blind image denoising. The AirNet [47] adopts the concept of contrast learning [48] to recover images from multiple types of degradation. The VDIR [49] utilizes variational framework for image restoration tasks. One popular and effective way to realize blind denoising is to equip a denoising model with a noise estimation sub-network, which usually is a convolution neural network has a simple structure, aiming to obtain the noise distributions in an image automatically. The noise estimation network of the CBDNet [32] and VDN [34] adopts a 5-layer fully convolutional network, the convolution kernel sizes are  $3 \times 3 \times 32$  and  $3 \times 3 \times 64$ , respectively. Neither the pooling nor batch normalization operations are used in their noise estimation network. The noise estimator of the BUIFD [33] consists of a 7-layer fully convolutional network with a convolution kernel of  $5 \times 5 \times 64$ , where the pooling is also not used, while the batch normalization is applied.

U-Net [41] was originally designed for semantic segmentation of multi-scale features, and later was utilized in the field of image denoising. A residual dense U-Net neural network (RDUNet) was presented in [44], which employs densely connected convolutional layers to reuse the feature maps, the local and global residual learning is used to avoid the gradient vanishing and accelerate the network training. Jia et al. [45] proposed a multi-scale cascaded U-Nets architecture called the Dense U-Net (DDUNet) for image denoising. The multi-scale dense skip connections are used for feature superposing across the cascading U-Nets, which promotes feature recycling and avoids the gradient vanishing. The DRUNet [31] utilizes the combination of the U-Net [41] and ResNet [38] as its model structure, and the state-of-the-art denoising performance was reported. The success of these U-Net based denoising models has demonstrated that U-Net can be an effective tool for image denoising.

Dilated convolution was first employed for wavelet decomposition [50]. Later, Yu et. al. [40] proposed a multi-scale context aggregation network for image segmentation based on dilated convolutions, and promising results have been obtained. The dilated convolution has the ability to enlarge the receptive field, a bigger receptive field can let the model extract more context information, therefore to promote the learning ability. Many denoising models have incorporated dilated convolutions in their networks. For instance, Zhang et al. [42] designed an image restoration CNN (IRCNN) for image blind denoising, image deblurring, and single image super-resolution. The hybrid dilated filters [51, 52] are utilized in IRCNN to enlarge the receptive field and address the gridding phenomenon. Following IRCNN, a dilated residual network (DSNet) [43] uses symmetric skip connections to further improve the denoising performance. The lower branch of the BRDNet [36] also adopts dilated convolutions to capture more context information.

Skip connection [38, 39] is generally used for tackling the problem of gradient vanishing or exploding during back-propagating. DnCNN [27] only uses one skip connection to obtain the denoised image. Mao et al. [53] proposed a very deep residual encoder-decoder network called the RED-Net for image restoration, where the skip connections are used to facilitate network training. A lightweight dense dilated fusion network (DDFN) was presented in [54, 55] for real-world image denoising, which tackles the vanishing or exploding of gradients by skip connections during network training. A single-stage blind real image denoising network (RIDNet) was designed in [56], which contains the enhancement attention modules (EAM) with short and long skip connections to improve denoising performance. Anwar et al. [57] developed an identity enhanced residual denoising (IERD) network with short and long skip connections for image denoising. It can be seen that using skip connections can be helpful for model training. More importantly, the features from different layers can be fused through skip connections, therefore much more semantic and structural features in images can be preserved.

### 3. The proposed model

#### 3.1. Network architecture

Our proposed DCBDNet consists of a noise estimation network and a dual convolutional denoising network (CNN). The architecture of the proposed DCBDNet is shown in Fig. 1. The model contains two main sub-networks: a noise estimation network (the green dashed box in Fig. 1) and a dual CNN denoising network (the orange dashed box in Fig. 1). The noise level map in a noisy image is first obtained by the noise estimation network, and it will be fed into the dual CNN with the noisy image together to produce the denoised result. The proposed dual CNN contains a U-shaped upper branch, and a lower branch with dilated convolutions, skip connections are applied in both branches.

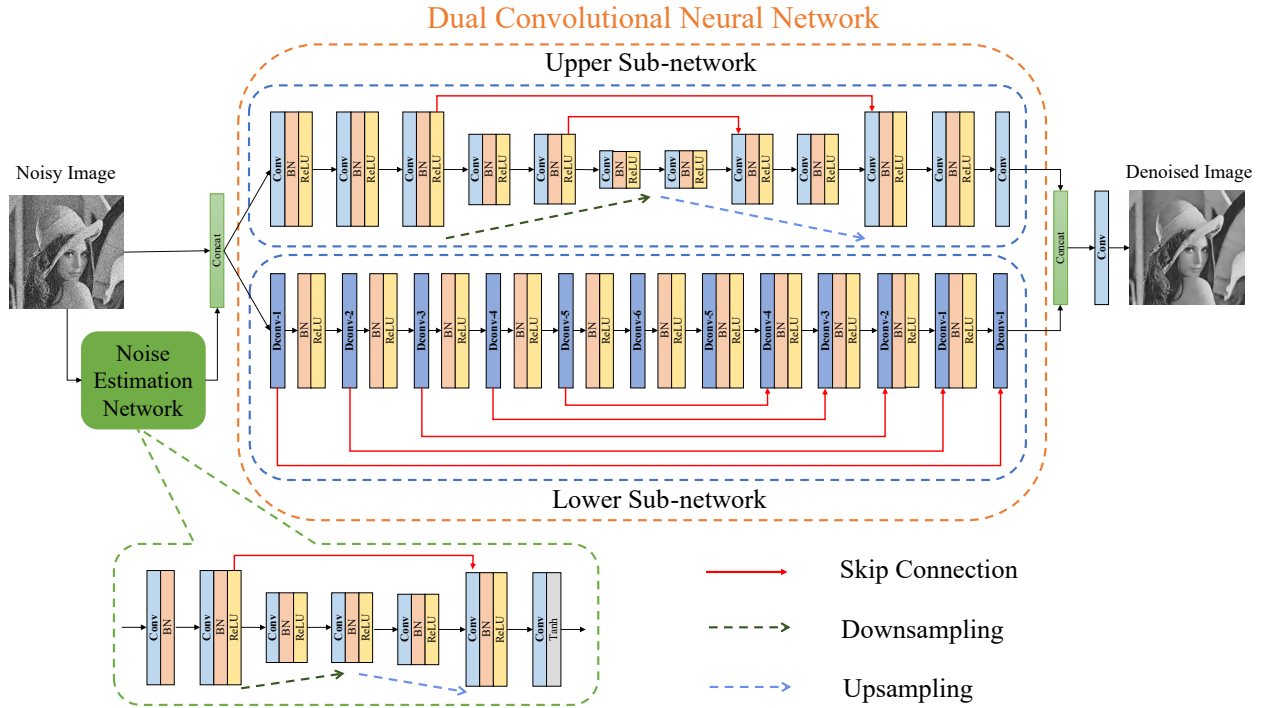


Figure 1: The network architecture of the proposed model for image denoising.

##### 3.1.1. Noise Estimation Network

To achieve image blind denoising, we use a noise estimation network to estimate the noise level map. In CBDNet [32] and VDN [34], an estimation network with 5 convolutional layers is used. In order to obtain a larger receptive

field, we design a noise estimation network with 7 convolutional layers, the convolutional kernel size is  $3 \times 3 \times 64$ .

Our noise estimation network consists of Conv, max-pooling (Downsampling) [58], bilinear interpolation (Upsampling) [59], batch normalization (BN) [60], rectified linear unit (ReLU) [61] and Tanh [62]. The downsampling and upsampling operations are utilized to enlarge its receptive field, which can extract more complex noise information and estimate the noise level map more accurately. As the downsampling operation may lead to a loss of image information, a skip connection is used in the network to reduce the loss.

It is apparent if the estimated noise level or noise distribution does not match the noise in the input image, the denoising performance will decline. In practice, people tend to estimate a high noise level to remove more noise, however if the estimated noise level is much higher than the real one, unwanted visual artifacts will be brought. As has been verified in [30, 31], the orthogonal initialization of the convolutional filters [63, 64, 65] is an effective way to solve this problem. Therefore the orthogonal initialization is also utilized in our network to obtain a balance between noise removal and image detail preservation.

### 3.1.2. Dual Convolutional Neural Network

Much previous work has verified that expanding the width of the network is also an effective way for improving network performance [66]. Therefore, we propose a dual CNN contains two parallel sub-networks to expand the width of the model, which contains an upper and a lower sub-networks. The upper sub-network contains standard convolution (Conv), max-pooling (Downsampling) [58], bilinear interpolation (Upsampling) [59], skip connections [38, 39], batch normalization (BN) [60], and rectified linear unit (ReLU) [61]. The lower sub-network comprises dilated convolution (DConv) [40], skip connection, BN, and ReLU. Different types of convolution filters allow the two sub-networks can extract complementary image features [67] and therefore enhance the generalization ability of the proposed DCBDNet.

Aiming for a desirable balance between network complexity and denoising performance, we set 12 convolutional layers for the upper and lower sub-networks respectively, and one convolutional layer after their concatenation. The convolutional filter size is set to  $3 \times 3 \times 64$  for both grayscale and color images. Moreover, in order to obtain similar sizes of the receptive fields in the two sub-networks and reduce the computational cost of the upper sub-network, different from the standard U-Net, in our dual CNN only two downsampling and upsampling operations are used. Since the downsampling operations will lead to the loss of image information, two skip connections are applied for feature superposing in the upper sub-network. Furthermore, symmetric skip connections are employed in the lower sub-network to accelerate its training and improve its detail preservation. The skip connections can also avoid the gradient vanishing or exploding for back-propagating during the network training.

The downsampling in the upper sub-network and the dilated convolutions in the lower sub-network aim to widen the receptive field and keep the sizes of the receptive fields in both two sub-networks close, which can obtain more image context and detail features. Inspired by the hybrid dilated convolution (HDC) [51, 52], we employ different dilated rates for each dilated convolution layer, and the rate in each layer is set to 1, 2, 3, 4, 5, 6, 5, 4, 3, 2, 1, 1, which can eliminate the gridding phenomenon and enhance the denoising performance [52]. The receptive fields of upper and lower sub-networks in different layers are listed in Table 1. It can be found that the two sub-networks own approximately the same size of receptive fields in the last layer. Specifically, if the receptive fields of two sub-networks have a large difference, it will lead to an increase in the computational cost of one sub-network, simultaneously the other sub-network may not extract enough image information due to the size limitation of its receptive fields, which may result in degradation of denoising performance.

Table 1: The receptive fields of the upper and lower sub-networks in different layers.

Layer	1	2	3	4	5	6	7	8	9	10	11	12
Upper sub-network	30	34	38	48	56	74	90	106	122	138	154	170
Lower sub-network	30	38	50	66	86	110	130	146	158	166	170	174

### 3.2. Loss function

In this subsection, we discuss the loss function of the proposed DCBDNet. To train the network parameters of the proposed DCBDNet for the AWGN removal, we select the average mean-square error (MSE) as the optimization

target, which is the most widely used optimization function. The loss function is defined in Eqn. (1).

$$\begin{aligned}\mathcal{L}(\theta) &= \frac{1}{2K} \sum_{j=1}^K \|\mathcal{F}(y_j; \theta) - x_j\|^2 \\ &= \frac{1}{2K} \sum_{j=1}^K \|\hat{x} - x_j\|^2,\end{aligned}\tag{1}$$

where  $x_j$ ,  $\hat{x}$ , and  $y_j$  represent the clean, predicted, and noisy images, respectively.  $\theta$  is the trainable network parameters, and  $K$  is the number of clean-noisy image patches.

For the real noise with spatial variation, using MSE as a loss function will produce a blurry and over-smoothed visual effect, and the high-frequency textures may be lost due to the square penalty. Therefore, the Charbonnier loss [68] is chosen as the reconstruction loss to optimize our DCBDNet. Moreover, to further enhance the fidelity and authenticity of high-frequency details when removing noise, following [69], we employ an edge loss to constrain the high-frequency components between the ground-truth image  $x$  and the denoised image  $\hat{x}$ . As our proposed DCBDNet includes a noise estimation network to estimate the noise level map  $\sigma(y)$  in the noisy image  $y$ , referring to [32], we adopt a total variation (TV) regularizer to constrain the smoothness of the estimated noise level. In summary, the overall loss function of our DCBDNet is defined as:

$$\mathcal{L} = \mathcal{L}_{char}(\hat{x}, x) + \lambda_{edge} \mathcal{L}_{edge}(\hat{x}, x) + \lambda_{TV} \mathcal{L}_{TV}(\sigma(y)),\tag{2}$$

where  $\lambda_{edge}$  and  $\lambda_{TV}$  empirically are set to 0.1 and 0.05, respectively.  $\mathcal{L}_{char}$  stands for the Charbonnier loss, which is defined as:

$$\mathcal{L}_{char} = \sqrt{\|\hat{x} - x\|^2 + \epsilon^2},\tag{3}$$

where the constant  $\epsilon$  is set as  $10^{-3}$ . The edge loss  $\mathcal{L}_{edge}$  is designed as:

$$\mathcal{L}_{edge} = \sqrt{\|\Delta(\hat{x}) - \Delta(x)\|^2 + \epsilon^2},\tag{4}$$

where  $\Delta$  denotes the Laplacian operator [70].  $\mathcal{L}_{TV}$  is defined as:

$$\mathcal{L}_{TV} = \|\nabla_h \sigma(y)\|_2^2 + \|\nabla_v \sigma(y)\|_2^2,\tag{5}$$

where  $\nabla_h(\nabla_v)$  is the gradient operator along the horizontal (vertical) direction.

## 4. Experiments and results

### 4.1. Datasets

For the AWGN removal, the DIV2K dataset [71] is used for our DCBDNet training, the dataset contains 800 high-resolution color images as training data, and 100 high-resolution color images for validation. The size of the training images in DIV2K was re-scaled to  $512 \times 512$ , and the images were grayscaled for training the grayscale image denoising model. The training images were randomly cropped into image patches. As the patch size is extremely important for the network training, based on the architecture of our proposed DCBDNet, the size of the image patches used in our experiments is set to  $180 \times 180$ . Since a noise estimation network and two sub-networks are contained in our proposed DCBDNet, the size of the receptive field of the upper sub-network is 170, and 174 for the lower sub-network.

In general, the size of image patches should be larger than the receptive fields of convolution layers, therefore the patch size of  $180 \times 180$  is appropriate for our DCBDNet training, for both grayscale images and color images. The patch size used here is larger than the patch sizes used in many other denoising models, which are usually set as  $50 \times 50$ , however our experimental results illustrate that due to the larger patch size, the proposed DCBDNet can capture more image context features for improving denoising performance, especially for the images contain high

noise levels. The AWGN in the noise level range of [0, 75] was added to each clean image patch to obtain noisy image patches.

The Set12 and BSD68 datasets [72] were used for our grayscale image denoising evaluation. The CBSD68 [72], Kodak24 [73] and McMaster [74] datasets were selected for the evaluation of color image denoising. For real image denoising, the training data of the SIDD[75] and RENOIR [76] datasets are selected for our model training. The SIDD training data contains 320 pairs of noisy images and the near noise-free counterparts. The RENOIR dataset is composed of 240 pairs of noisy images and the near noise-free counterparts. In order to facilitate network training, the images in these two datasets were randomly cropped into image patches of size  $180 \times 180$ . Moreover, the rotation and flipping operations were used for data augmentation. The SIDD validation set, DND sRGB images [77], RNI15 [78] and Nam [79] datasets were used for evaluation. We also validated the effectiveness of our model on the Set5 dataset [80] for spatially variant noise.

#### 4.2. Experimental settings

All our experiments were implemented on a computer with a sixteen-core Intel(R) Core(TM) i7-11700KF CPU @ 2.50GHz, 32 GB of RAM, and an NVIDIA GeForce RTX 3080Ti GPU. The proposed DCBDNet for grayscale and color images were trained respectively. It costs about 42 hours to complete DCBDNet training. For the DCBDNet model of real denoising, it takes about 50 hours to train our model.

The model parameters are optimized by the Adam optimizer [81]. For the AWGN removal, the DCBDNet was trained for 700,000 iterations, during which the initial learning rate is  $10^{-4}$  and then decreases by half every 100,000 iterations. For real image denoising, we applied 120 epochs to train the DCBDNet model, during which the initial learning rate is  $2 \times 10^{-4}$  and is steadily reduced to  $10^{-6}$  using cosine annealing strategy [82]. The batch size was set to 16. For other hyper-parameters of the Adam algorithm, we used the default settings.

#### 4.3. Ablation study

In order to validate the effectiveness of our proposed network architecture, especially the effects of the skip connection, we trained four different networks for grayscale and color image denoising, respectively. The models under the combinations of with/without skip connection and with/without batch normalization (BN) were trained and tested. The four different models and their corresponding performances can be seen in Fig. 2. The Set12 [72] and Kodak24 [73] datasets were used for grayscale and color image denoising evaluation, respectively. The noise level was set to 25, and the averaged PSNR on each 10,000 iterations was recorded.

In Fig. 2, it can be seen that the denoising network with skip connection and BN achieves a better denoising performance than the other three networks on both grayscale images and color images. The results have verified that using skip connection and BN in the denoising network can enhance its performance.

#### 4.4. Denoising Evaluation

We evaluated the denoising performance of our DCBDNet model quantitatively and qualitatively. For quantitative analysis, we calculate the peak signal-to-noise ratio (PSNR), structural similarity index measure (SSIM) [83], feature similarity index measure (FSIM) [84], the learned perceptual image patch similarity (LPIPS) as well as the DeepFeatures [85] and Inception-Score [86]. For qualitative evaluation, we compared the visual effect of the denoised images from different methods.

#### 4.5. Evaluation of spatially invariant AWGN removal

We first present the results of the spatially invariant AWGN removal on grayscale images. Table 2 reports the PSNR values at different noise levels for the compared denoising methods on the Set12 dataset. It can be seen that the denoising performance of our proposed DCBDNet is slightly inferior to the DeamNet and DRUNet. However, the DeamNet and DRUNet are both equipped with complex network structures. The performance of the proposed DCBDNet is lower than the denoising results of the BRDNet on the noise levels of 15 and 25, but higher than BRDNet when the noise level is 50, which indicates that our DCBDNet is more robust for the images with high noise levels. More importantly, our proposed DCBDNet has a more compact network than BRDNet.

It should be noted that the WNNM obtained excellent denoising performances under different noise levels on the image “Barbara”. There are rich repetitive structures exist in this image, and they can be effectively learned by the

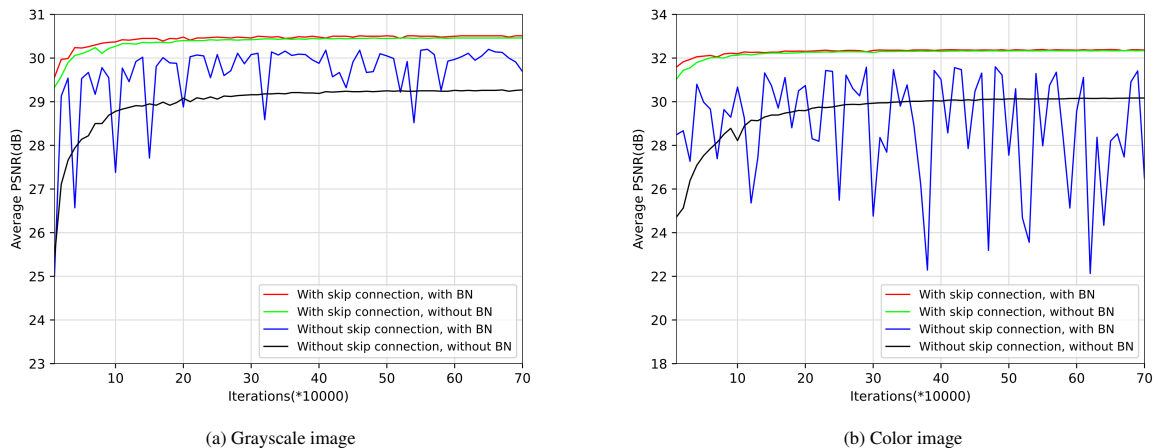


Figure 2: Ablation study results of the proposed model. The average PSNR(dB) of four various network architectures on Set12 and Kodak24 datasets were recorded at noise level 25 during different iterations.

methods like WNNM which is based on non-local self-similarity learning. One can also see that the performance of TID is unsatisfied under all tested noise levels, as TID works well only on the specific datasets which contain images have similar image patches, however the Set12 dataset does not meet the above condition.

Table 3 shows the averaged SSIM on the Set12 dataset for the compared denoising methods. It can be seen that our DCBDNet obtains competitive performance, the DeamNet and DRUNet obtain the leading results, however the DRUNet uses a manually pre-defined noise level map to obtain the results, and both the DeamNet and DRUNet have much deeper network structure than our model.

Table 4 and Table 5 list the averaged PSNR and SSIM results on the BSD68 dataset for the compared denoising methods, respectively. Table 6 lists the average FSIM on the Set12 and BSD68 datasets of the compared denoising methods. One can see that our DCBDNet model obtains competitive denoising performance.

Fig. 3 shows the denoised results on the “Castle” image from the BSD68 dataset at the noise level 50 of different methods. In Fig. 3, we zoom in a region (green box) for detail comparison (red box). It can be seen that though the DeamNet and DRUNet achieve high PSNRs, the ‘over-smooth’ effects are also brought. The DeamNet completely replaces the white small region (not noise) with the image context (Fig. 3 (h)), and the DRUNet changes the original irregular white region into a regular one (Fig. 3 (i)), while our proposed method can maintain a balance between noise removal and detail preservation (Fig. 3 (j)).

To evaluate the denoising performance of AWGN removal on color images, the CBS68, Kodak24, and McMaster datasets were used. The PSNR values obtained by the compared methods are listed in Table 7. It can be seen that our proposed DCBDNet outperforms all the compared methods except the DRUNet on CBS68, Kodak24, and McMaster datasets at noise levels 50 and 75. The proposed DCBDNet outperforms the BRDNet on the three datasets when the noise level is greater than 35. As the BRDNet also employs a dual CNN structure, we think the reason is a deeper network structure like the one used in the BRDNet may have more learning ability when the noise power is not strong.

Table 8 shows the averaged SSIM, FSIM, LPIPS, and the Inception-Score (IS) results of different methods on CBS68, Kodak24, and McMaster datasets. Our DCBDNet model outperforms DnCNN, IRCNN, and FFDNet on the four evaluation metrics.

The visual results of color image AWGN removal at noise level 50 can be seen in Fig. 4, where the “kodim22” image from the Kodak24 dataset is used. It can be seen that the small white dot in the red box is overly smoothed by CBM3D and AirNet, while it is well preserved by our DCBDNet.

#### 4.6. Spatially variant AWGN removal

We follow the same technique in FFDNet [30] to obtain the additive white Gaussian noise (AWGN) with spatial variation, the bivariate Gaussian probability density function is used to simulate a spatial variant noise distribution, as



Table 2: The PSNR (dB) results of the compared methods on the Set12 dataset with different noise levels. The best, second best and third best are emphasized in red, blue and green respectively.

Images	C.man	House	Peppers	Starfish	Monar.	Airpl.	Parrot	Lena	Barbara	Boat	Man	Couple	Average
Noise level	$\sigma=15$												
BM3D [6]	31.91	34.93	32.69	31.14	31.85	31.07	31.37	34.26	33.10	32.13	31.92	31.10	32.37
WNNM [23]	32.17	35.13	32.99	31.82	32.71	31.39	31.62	34.27	<b>33.60</b>	32.27	32.11	32.17	32.70
GNLM [3]	-	35.01	32.98	-	-	-	-	33.89	-	31.69	31.94	-	-
TID [5]	24.32	29.29	24.93	23.88	24.96	24.30	23.75	28.92	23.62	26.20	27.56	26.52	25.69
TNRD [26]	32.19	34.53	33.04	31.75	32.56	31.46	31.63	34.24	32.13	32.14	32.23	32.11	32.50
DnCNN-S [27]	32.61	34.97	33.30	32.20	33.09	31.70	31.83	34.62	32.64	32.42	32.46	32.47	32.86
BUIFD [33]	31.74	34.78	32.80	31.92	32.77	31.34	31.39	34.38	31.68	32.18	32.25	32.22	32.46
IRCNN [42]	32.55	34.89	33.31	32.02	32.82	31.70	31.84	34.53	32.43	32.34	32.40	32.40	32.77
FFDNet [30]	32.43	35.07	33.25	31.99	32.66	31.57	31.81	34.62	32.54	32.38	32.41	32.46	32.77
BRDNet [36]	32.80	<b>35.27</b>	<b>33.47</b>	32.24	<b>33.35</b>	31.85	<b>32.00</b>	<b>34.75</b>	32.93	32.55	<b>32.50</b>	<b>32.62</b>	<b>33.03</b>
ADNet [87]	<b>32.81</b>	35.22	<b>33.49</b>	32.17	33.17	<b>31.86</b>	31.96	34.71	32.80	<b>32.57</b>	32.47	32.58	32.98
DudeNet [37]	32.71	35.13	33.38	<b>32.29</b>	33.28	31.78	31.93	34.66	32.73	32.46	32.46	32.49	32.94
DeamNet [46]	<b>32.82</b>	<b>35.77</b>	<b>33.47</b>	<b>32.55</b>	<b>33.57</b>	<b>31.94</b>	<b>32.05</b>	<b>34.94</b>	<b>33.21</b>	<b>32.67</b>	<b>32.56</b>	<b>32.73</b>	<b>33.19</b>
DRUNet [31]	<b>32.91</b>	<b>35.83</b>	<b>33.56</b>	<b>32.44</b>	<b>33.61</b>	<b>31.99</b>	<b>32.13</b>	<b>34.93</b>	<b>33.44</b>	<b>32.71</b>	<b>32.61</b>	<b>32.78</b>	<b>33.25</b>
DCBDNet	32.14	35.05	33.01	32.06	33.09	31.50	31.66	34.68	32.57	32.41	32.39	32.43	32.75
Noise level	$\sigma=25$												
BM3D [6]	29.45	32.85	30.16	28.56	29.25	28.42	28.93	32.07	30.71	29.90	29.61	29.71	29.97
WNNM [23]	29.64	33.22	30.42	29.03	29.84	28.69	29.15	32.24	<b>31.24</b>	30.03	29.76	29.82	30.26
GNLM [3]	-	32.91	30.19	-	-	-	-	31.67	-	29.71	29.63	-	-
TID [5]	24.17	28.65	24.64	23.53	24.74	23.92	23.56	28.30	23.37	25.83	27.04	26.03	25.32
TNRD [26]	29.72	32.53	30.57	29.02	29.85	28.88	29.18	32.00	29.41	29.91	29.87	29.71	30.06
DnCNN-S [27]	30.18	33.06	30.87	29.41	30.28	29.13	29.43	32.44	30.00	30.21	30.10	30.12	30.43
BUIFD [33]	29.42	33.03	30.48	29.21	30.20	28.99	28.94	32.20	29.18	29.97	29.88	29.90	30.12
IRCNN [42]	30.08	33.06	30.88	29.27	30.09	29.12	29.47	32.43	29.92	30.17	30.04	30.08	30.38
FFDNet [30]	30.10	33.28	30.93	29.32	30.08	29.04	29.44	32.57	30.01	30.25	30.11	30.20	30.44
BRDNet [36]	<b>31.39</b>	<b>33.41</b>	31.04	29.46	<b>30.50</b>	<b>29.20</b>	<b>29.55</b>	32.65	30.34	30.33	<b>30.14</b>	<b>30.28</b>	<b>30.61</b>
ADNet [87]	30.34	<b>33.41</b>	<b>31.14</b>	29.41	30.39	29.17	29.49	32.61	30.25	<b>30.37</b>	30.08	30.24	30.58
DudeNet [37]	30.23	33.24	30.98	<b>29.53</b>	30.44	29.14	29.48	32.52	30.15	30.24	30.08	30.15	30.52
DeamNet [46]	<b>30.41</b>	<b>33.79</b>	<b>31.13</b>	<b>29.92</b>	<b>30.75</b>	<b>29.32</b>	<b>29.62</b>	<b>32.90</b>	<b>30.76</b>	<b>30.51</b>	<b>30.20</b>	<b>30.46</b>	<b>30.81</b>
DRUNet [31]	<b>30.61</b>	<b>33.92</b>	<b>31.22</b>	<b>29.88</b>	<b>30.89</b>	<b>29.35</b>	<b>29.72</b>	<b>32.97</b>	<b>31.23</b>	<b>30.58</b>	<b>30.30</b>	<b>30.56</b>	<b>30.94</b>
DCBDNet	30.07	33.27	30.74	29.46	30.44	29.05	29.42	<b>32.70</b>	30.29	30.31	30.12	30.21	30.51
Noise level	$\sigma=50$												
BM3D [6]	26.13	29.69	26.68	25.04	25.82	25.10	25.90	29.05	27.22	26.78	26.81	26.46	26.72
WNNM [23]	26.45	30.33	26.95	25.44	26.32	25.42	26.14	29.25	<b>27.79</b>	26.97	26.94	26.64	27.05
GNLM [3]	-	28.99	26.96	-	-	-	-	28.49	-	26.63	26.78	-	-
TID [5]	23.39	27.00	23.73	22.49	23.43	23.03	22.75	26.89	22.80	24.76	25.72	24.87	24.24
TNRD [26]	26.62	29.48	27.10	25.42	26.31	25.59	26.16	28.93	25.70	26.94	26.98	26.50	26.81
DnCNN-S [27]	27.03	30.00	27.32	25.70	26.78	25.87	26.48	29.39	26.22	27.20	27.24	26.90	27.18
BUIFD [33]	25.44	29.76	26.50	24.87	26.49	25.34	25.07	28.81	25.49	26.59	26.87	26.34	26.46
IRCNN [42]	26.88	29.96	27.33	25.57	26.61	25.89	26.55	29.40	26.24	27.17	27.17	26.88	27.14
FFDNet [30]	27.05	30.37	27.54	25.75	26.81	25.89	26.57	29.66	26.45	27.33	27.29	27.08	27.32
BRDNet [36]	<b>27.44</b>	30.53	27.67	25.77	26.97	<b>25.93</b>	<b>26.66</b>	25.93	26.66	27.38	27.27	<b>27.17</b>	27.45
ADNet [87]	27.31	<b>30.59</b>	<b>27.69</b>	25.70	26.90	25.88	26.56	29.59	26.64	27.35	27.17	27.07	27.37
DudeNet [37]	27.22	30.27	27.51	25.88	26.93	25.88	26.50	29.45	26.49	27.26	27.19	26.97	27.30
DeamNet [46]	<b>27.44</b>	<b>31.19</b>	<b>27.78</b>	<b>26.48</b>	<b>27.19</b>	<b>26.08</b>	<b>26.72</b>	<b>29.96</b>	<b>27.62</b>	<b>27.61</b>	<b>27.38</b>	<b>27.45</b>	<b>27.74</b>
DRUNet [31]	<b>27.80</b>	<b>31.26</b>	<b>27.87</b>	<b>26.49</b>	<b>27.31</b>	<b>26.08</b>	<b>26.92</b>	<b>30.15</b>	<b>28.16</b>	<b>27.66</b>	<b>27.46</b>	<b>27.59</b>	<b>27.90</b>
DCBDNet	<b>27.35</b>	30.45	27.50	<b>25.91</b>	<b>27.01</b>	<b>25.94</b>	26.63	<b>29.78</b>	27.10	<b>27.39</b>	<b>27.30</b>	27.14	<b>27.46</b>

Table 3: The averaged SSIM results of the compared methods on Set12 dataset with different noise levels. The best, second best and third best is highlighted in red, blue and green, respectively.

Noise level	$\sigma=15$	$\sigma=25$	$\sigma=50$
BM3D [6]	0.896	0.851	0.766
WNNM [23]	0.894	0.846	0.756
TNRD [26]	0.896	0.851	0.768
DnCNN-S [27]	0.903	0.862	0.783
BUIFD [33]	0.899	0.855	0.755
IRCNN [42]	0.901	0.860	0.780
FFDNet [30]	0.903	0.864	0.791
BRDNet [36]	0.906	0.866	0.794
ADNet [87]	0.905	0.865	0.791
RIDNet [56]	0.906	0.867	0.793
CDNet [88]	0.903	0.865	0.792
DeamNet [46]	0.910	0.872	0.806
DRUNet [31]	0.910	0.873	0.810
DCBDNet	0.902	0.865	0.794

Table 4: The averaged PSNR (dB) results of the compared methods on BSD68 dataset with different noise levels. The best, second best and third best is highlighted in red, blue and green, respectively.

Methods	$\sigma=15$	$\sigma=25$	$\sigma=35$	$\sigma=50$	$\sigma=75$
BM3D [6]	31.07	28.57	27.08	25.62	24.21
WNNM [23]	31.37	28.83	27.30	25.87	24.40
TNRD [26]	31.42	28.92	-	25.97	-
DnCNN-S [27]	31.72	29.23	27.69	26.23	24.64
BUIFD [33]	31.35	28.75	27.03	25.11	22.68
IRCNN [42]	31.63	29.15	27.66	26.19	-
FFDNet [30]	31.63	29.19	27.73	26.29	24.79
DSNetB [43]	31.69	29.22	-	26.29	-
RIDNet [56]	31.81	29.34	-	26.40	-
BRDNet [36]	31.79	29.29	-	26.36	-
ADNet [87]	31.74	29.25	-	26.29	-
DudeNet [37]	31.78	29.29	-	26.31	-
CDNet [88]	31.74	29.28	27.77	26.36	24.85
DeamNet [46]	31.91	29.44	-	26.54	-
DRUNet [31]	31.91	29.48	28.02	26.59	25.10
DCBDNet	31.65	29.24	27.80	26.37	24.86

Table 5: The averaged SSIM results of the compared methods on BSD68 dataset with different noise levels. The best, second best and third best is highlighted in red, blue and green respectively.

Noise level	$\sigma=15$	$\sigma=25$	$\sigma=50$
BM3D [6]	0.872	0.802	0.687
WNNM [23]	0.878	0.810	0.698
TNRD [26]	0.883	0.816	0.703
DnCNN-S [27]	0.891	0.828	0.719
BUIFD [33]	0.886	0.819	0.682
IRCNN [42]	0.888	0.825	0.717
FFDNet [30]	0.890	0.830	0.726
BRDNet [36]	0.893	0.831	0.727
ADNet [87]	0.892	0.829	0.722
RIDNet [56]	0.893	0.833	0.727
CDNet [88]	0.892	0.831	0.727
DeamNet [46]	0.896	0.837	0.737
DRUNet [31]	0.895	0.837	0.738
DCBDNet	0.889	0.829	0.727

Table 6: The averaged FSIM results of the compared methods on Set12 and BSD68 dataset with different noise levels.

Datasets	Methods	$\sigma=15$	$\sigma=25$	$\sigma=50$
Set12	DnCNN-S [27]	0.761	0.719	0.655
	DnCNN-B [27]	0.759	0.720	0.656
	IRCNN [42]	0.759	0.718	0.656
	FFDNet [30]	0.760	0.719	0.656
	DRUNet [31]	0.768	0.727	0.666
	DCBDNet	0.760	0.722	0.662
	BSD68	DnCNN-S [27]	0.746	0.689
DnCNN-B [27]		0.744	0.688	0.601
IRCNN [42]		0.742	0.686	0.602
FFDNet [30]		0.745	0.690	0.602
DRUNet [31]		0.750	0.696	0.612
DCBDNet		0.746	0.692	0.609

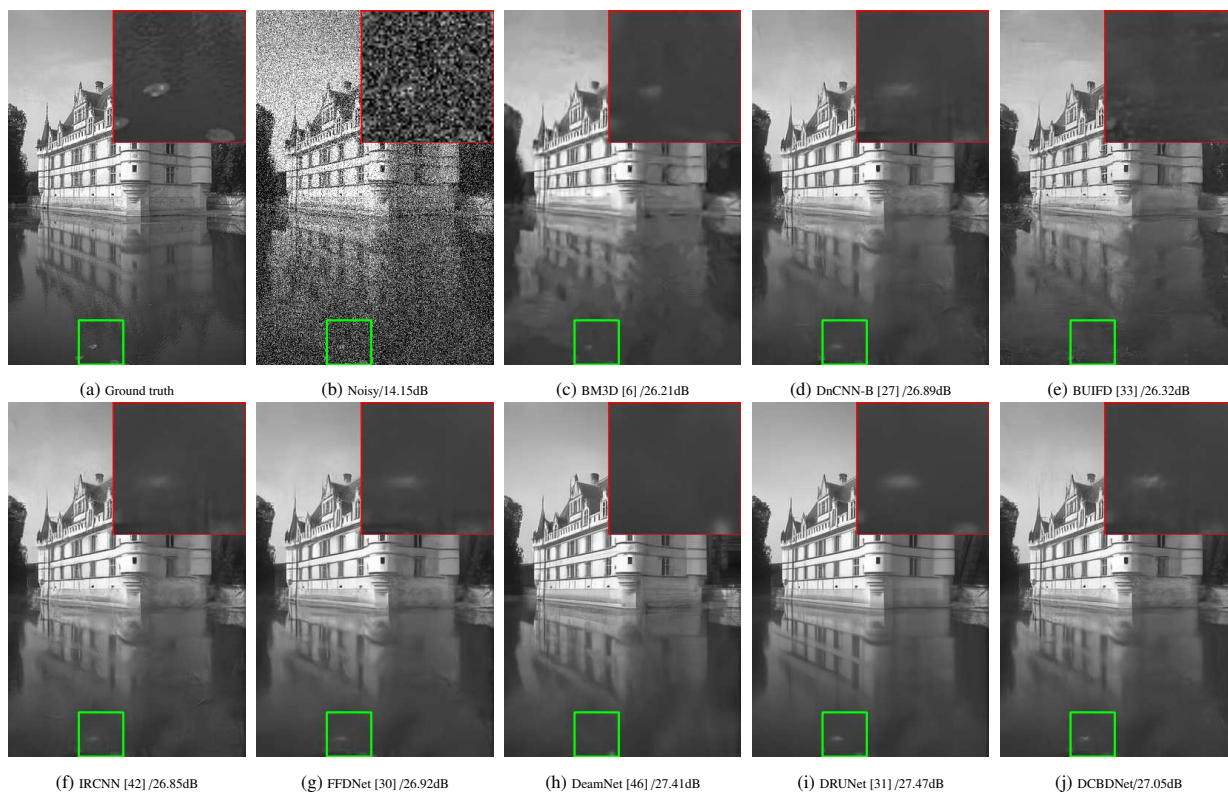


Figure 3: Visual results on the image “Castle” of different denoising methods.

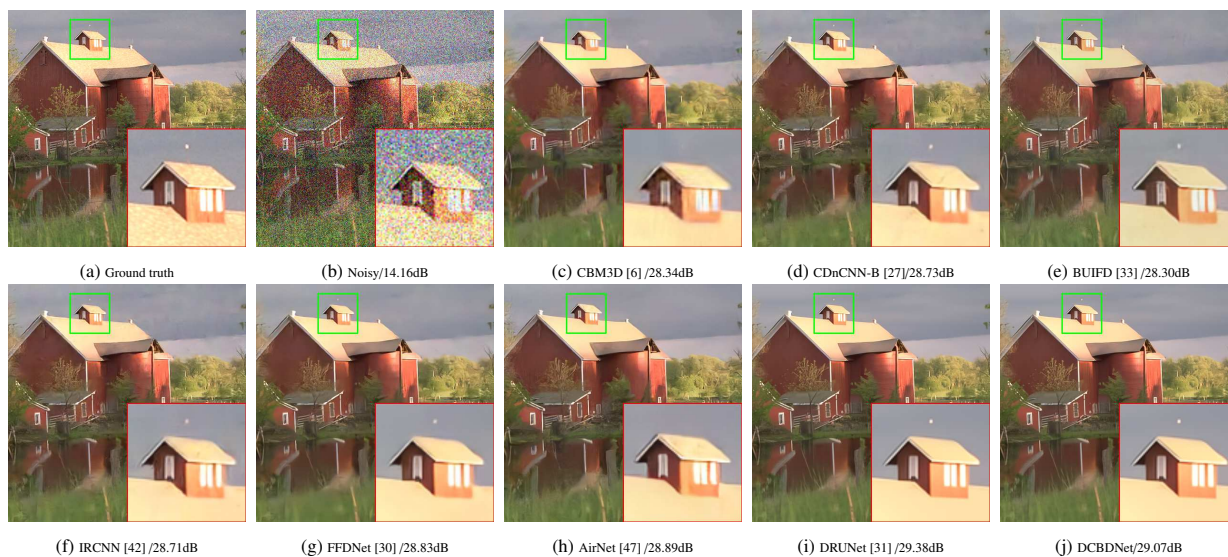


Figure 4: Visual results on the image “kodim22” from Kodak24 dataset.

Table 7: The averaged PSNR (dB) of the compared methods on the CBSD68, Kodak24 and McMaster datasets. The best, second best and third best is marked in red, blue and green respectively.

Datasets	Methods	$\sigma=15$	$\sigma=25$	$\sigma=35$	$\sigma=50$	$\sigma=75$
CBSD68	CBM3D [6]	33.52	30.71	28.89	27.38	25.74
	MCWNNM [24]	30.91	27.61	25.88	23.18	21.21
	CDnCNN-S [27]	33.89	31.23	29.58	27.92	24.47
	BUIFD [33]	33.65	30.76	28.82	26.61	23.64
	IRCNN [42]	33.86	31.16	29.50	27.86	-
	FFDNet [30]	33.87	31.21	29.58	27.96	26.24
	DSNetB [43]	33.91	31.28	-	28.05	-
	RIDNet [56]	34.01	31.37	-	28.14	-
	VDN [34]	33.90	31.35	-	28.19	-
	BRDNet [36]	34.10	31.43	29.77	28.16	26.43
	ADNet [87]	33.99	31.31	29.66	28.04	26.33
	DudeNet [37]	34.01	31.34	29.71	28.09	26.40
	GradNet [89]	34.07	31.39	-	28.12	-
	CDNet [88]	-	31.34	29.84	28.14	-
	AirNet [47]	33.92	31.26	-	28.01	-
DRUNet [31]	34.30	31.69	30.09	28.51	26.84	
DCBDNet	34.01	31.41	29.81	28.22	26.54	
Kodak24	CBM3D [6]	34.28	31.68	29.90	28.46	26.82
	MCWNNM [24]	32.00	28.76	27.02	21.18	18.06
	CDnCNN-S [27]	34.48	32.03	30.46	28.85	25.04
	BUIFD [33]	34.41	31.77	29.94	27.74	24.67
	IRCNN [42]	34.56	32.03	30.43	28.81	-
	FFDNet [30]	34.63	32.13	30.57	28.98	27.27
	DSNetB [43]	34.63	32.16	-	29.05	-
	BRDNet [36]	34.88	32.41	30.80	29.22	27.49
	ADNet [87]	34.76	32.26	30.68	29.10	27.40
	DudeNet [37]	34.81	32.26	30.69	29.10	27.39
	GradNet [89]	34.85	32.35	-	29.23	-
	AirNet [47]	34.68	32.21	-	29.06	-
	DRUNet [31]	35.31	32.89	31.26	29.86	28.06
DCBDNet	34.80	32.38	30.84	29.29	27.60	
McMaster	CBM3D [6]	34.06	31.66	29.92	28.51	26.79
	MCWNNM [24]	32.75	29.39	27.44	21.37	18.16
	CDnCNN-S [27]	33.44	31.51	30.14	28.61	25.10
	BUIFD [33]	33.84	31.06	28.87	26.20	22.75
	IRCNN [42]	34.58	32.18	30.59	28.91	-
	FFDNet [30]	34.66	32.35	30.81	29.18	27.33
	DSNetB [43]	34.67	32.40	-	29.28	-
	BRDNet [36]	35.08	32.75	31.15	29.52	27.72
	ADNet [87]	34.93	32.56	31.00	29.36	27.53
	GradNet [89]	34.81	32.45	-	29.39	-
	AirNet [47]	34.70	32.44	-	29.26	-
	DRUNet [31]	35.40	33.14	31.66	30.08	28.29
	DCBDNet	34.76	32.56	31.10	29.54	27.75

Table 8: The averaged SSIM, FSIM, LPIPS and Inception-Score (IS) results of the compared methods on CBSD68, Kodak24 and McMaster datasets with different noise levels.

Datasets	Methods	$\sigma=15$				$\sigma=25$				$\sigma=50$			
		SSIM	FSIM	LPIPS	IS	SSIM	FSIM	LPIPS	IS	SSIM	FSIM	LPIPS	IS
CBSD68	CDnCNN-B [27]	0.929	0.784	0.0628	4.354	0.883	0.737	0.1090	4.250	0.790	0.658	0.2101	4.064
	IRCNN [42]	0.929	0.782	0.0626	4.330	0.882	0.736	0.1078	4.243	0.790	0.660	0.2039	4.189
	FFDNet [30]	0.929	0.782	0.0655	4.270	0.882	0.733	0.1210	4.166	0.789	0.648	0.2442	3.946
	DRUNet [31]	0.934	0.791	0.0556	4.314	0.893	0.748	0.0962	4.259	0.810	0.675	0.1815	4.097
	DCBDNet	0.931	0.785	0.0604	4.330	0.887	0.740	0.1036	4.273	0.780	0.665	0.1994	4.054
Kodak24	CDnCNN-B [27]	0.920	0.765	0.0828	2.003	0.876	0.713	0.1292	1.965	0.791	0.632	0.2290	1.917
	IRCNN [42]	0.920	0.764	0.0810	1.989	0.877	0.712	0.1270	1.977	0.793	0.634	0.2202	1.931
	FFDNet [30]	0.922	0.764	0.0846	1.988	0.878	0.709	0.1395	1.947	0.794	0.621	0.2553	1.933
	DRUNet [31]	0.929	0.777	0.0688	2.021	0.891	0.730	0.1081	1.971	0.820	0.655	0.1862	1.874
	DCBDNet	0.924	0.770	0.0762	2.009	0.884	0.721	0.1182	1.961	0.806	0.644	0.2064	1.907
McMaster	CDnCNN-B [27]	0.904	0.759	0.0684	1.488	0.869	0.723	0.1014	1.441	0.799	0.662	0.1725	1.457
	IRCNN [42]	0.920	0.770	0.0608	1.485	0.882	0.730	0.0935	1.450	0.807	0.668	0.1567	1.458
	FFDNet [30]	0.922	0.769	0.0648	1.505	0.886	0.731	0.1026	1.465	0.815	0.668	0.1832	1.458
	DRUNet [31]	0.932	0.781	0.0512	1.472	0.903	0.746	0.0812	1.458	0.846	0.689	0.1403	1.445
	DCBDNet	0.923	0.772	0.0599	1.487	0.891	0.737	0.0909	1.472	0.828	0.679	0.1558	1.435

shown in Eqn. (6).

$$\begin{aligned}
 p = & 3(1 - m)^2 e^{-(m^2 - (n+1)^2)} \\
 & - 10\left(\frac{m}{5} - m^3 - n^5\right) e^{-(m^2 - n^2)} \\
 & - \frac{1}{3} e^{-(m+1)^2 - n^2}.
 \end{aligned} \tag{6}$$

For an estimated spatially variant noise distribution  $p$ , the non-uniform noise level map  $M$  can be obtained by Eqn. (7).

$$M = \lambda \frac{p - \min(p)}{\max(p) - \min(p)}, \tag{7}$$

where the  $\lambda$  is a coefficient used to control the intensity of the noise.  $\lambda$  and the normalized distribution  $p$  are multiplied to generate the spatial variant noise level map. The spatially variant AWGN can be obtained by Eqn. (8).

$$N = M \cdot D, \tag{8}$$

where  $D$  is the standard normal distribution  $\mathcal{N}(0, 1)$ . The clean image  $x$  and the noise level  $N$  were then added at the element level to gain spatially variant AWGN image  $y$ , which is represented as  $y = x + N$ .

To verify the effectiveness of the proposed DCBDNet for spatially variant AWGN removal, we choose the ‘‘butterfly’’ image from the Set5 dataset for visual evaluation, and the  $\lambda$  in Eqn. (7) was set as 50. Fig. 5 shows the visual comparison of the compared methods. It can be seen that the DCBDNet and VDN are effective to eliminate the spatially variant AWGN.

#### 4.7. Real noisy image denoising evaluation

For the evaluation of the real noisy image denoising, the SIDD validation set, DND sRGB images, RNI15, and Nam datasets were used. The SIDD validation set, DND sRGB images, and Nam dataset contain noisy images and the near noise-free counterparts, the quantitative evaluation can be implemented. Table 9 lists the averaged PSNR and SSIM values of different methods on the SIDD validation set and DND sRGB images. One can see that our proposed DCBDNet model achieves more effective denoising performance than MCWNNM, TWSC, DnCNN-B, CBDNet, and RIDNet, however the VDN and VDIR outperform our model, however both of them have much more complex model structures than ours.

Fig. 6 shows the visual comparison from the compared denoising methods. It can be found the VDN, VDIR, and the proposed DCBDNet achieve better visual quality.

The RNI15 dataset consists of 15 real noisy images without the corresponding ground truth images, therefore the quantitative comparison can not be implemented. The visual results of the compared denoising models on the image

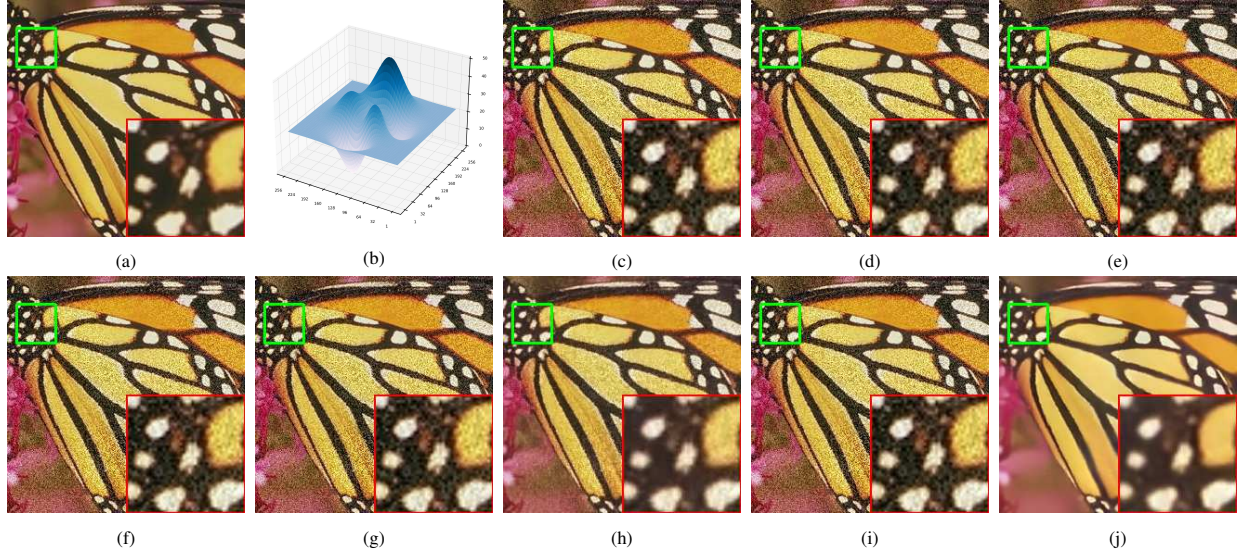


Figure 5: Visual results on the image “butterfly” from Set5 dataset with spatially variant AWGN. (a) Ground-truth image / (PSNR (dB) /SSIM), (b) Non-uniform noise level map, (c) Noisy image degraded by spatially variant AWGN / (20.74/0.552), (d) CDnCNN-B / (20.83/0.555), (e) ADNet / ((20.78/0.592), (f) BUIFD / (20.74/0.590), (g) AirNet / (20.64/0.586), (h) VDN / (24.72/0.743), (i) VDIR / (20.95/0.596), (j) DCBDNet / (23.85/0.847).

Table 9: The averaged PSNR(dB), SSIM and FSIM of different denoising methods on the SIDD validation set and DND sRGB images. The top three results on each noise level are marked in red, blue and green in order.

Dataset	Methods	MCWNNM [24]	TWSC [12]	DnCNN-B [27]	CBDNet [32]	RIDNet [56]	VDN [34]	VDIR [49]	DCBDNet
SIDD	PSNR	33.40	35.33	23.66	30.78	38.71	39.28	39.26	38.94
	SSIM	0.879	0.933	0.583	0.951	0.954	0.957	0.955	0.953
DND	PSNR	37.38	37.94	37.90	38.06	39.26	39.38	39.63	39.37
	SSIM	0.929	0.940	0.943	0.942	0.953	0.952	0.953	0.951

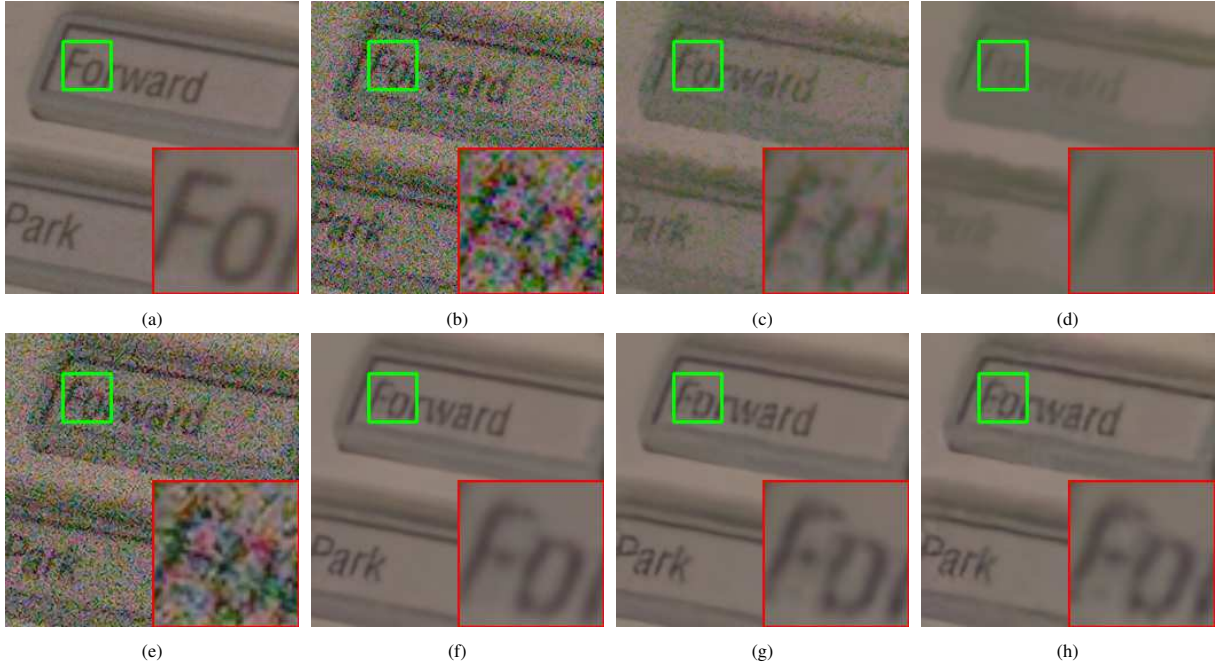


Figure 6: Visual results on the image “11.4” from SIDD the SIDD validation set. (a) Ground-truth image / (PSNR (dB) /SSIM), (b) Noisy image / (18.25/0.169), (c) MCWNNM / (28.63/0.702), (d) TWSC / (30.41/0.811), (e) CDnCNN-B / (20.76/0.235), (F) VDN / (36.39/0.907), (G) VDIR / (36.35/0.906), (h) DCBDNet / (35.61/0.906).

“Dog” can be seen in Fig. 7, where one can see that the TWSC, CDnCNN-B, VDN, and VDIR produced inferior visual results. Furthermore, the MCWNNM and the proposed DCBDNet obtained visual appealing results.

Fig. 8 displays the denoising results of the compared denoising methods on the image “Vinegar” from the Nam dataset, where one can see that the MCWNNM, TWSC, VDN, and the proposed DCBDNet obtained better visual quality and PSNR/SSIM values. It also should be noted that even nowadays the DNN based methods are much more popular in image denoising, however the traditional methods like the MCWNNM and TWSC still can obtain remarkable denoising performance in real denoising tasks.

#### 4.8. Network complexity analysis

In our experiments, the network complexity was evaluated from the perspectives of model running time, floating point operations per second (FLOPs), and numbers of network parameters. It should be noted that we used the original source codes of the compared denoising methods released by the authors, therefore the BM3D, WNNM, MCWNNM, and TWSC were implemented in Matlab (R2020a) environment, and the DnCNN-B, BUFD, IRCNN, FFDNet, BRDNet, ADNet, DudeNet, CBDNet, RIDNet, VDN, VDIR, DeamNet, AirNet, DRUNet, and the proposed DCBDNet were evaluated in PyCharm (2021) environment.

We first evaluated the running time of different denoising methods, the results are listed in Table 10. Three randomly chosen grayscale and color images with different sizes were utilized for evaluating the running time at noise level 25, and the running time on each image of every evaluated model was obtained by averaging the running time of 20 implementations. Our experiments neglected the memory transfer time between CPU and GPU. It can be observed that the denoising speed of BM3D, WNNM, MCWNNM, and TWSC using CPU is much slower than the methods running on GPU. The models can achieve leading PSNR values such as the DeamNet and DRUNet require a longer denoising time, especially when the size of the image is bigger. More importantly, these models equipped with complex structures also require much longer training time.

Table 11 lists the number of parameters and FLOPs of the tested denoising methods on grayscale and color images, respectively. For the network parameters, it can be seen that DnCNN-B, IRCNN, FFDNet, and ADNet have smaller numbers of parameters than our DCBDNet, however the quantitative results of our DCBDNet are superior to



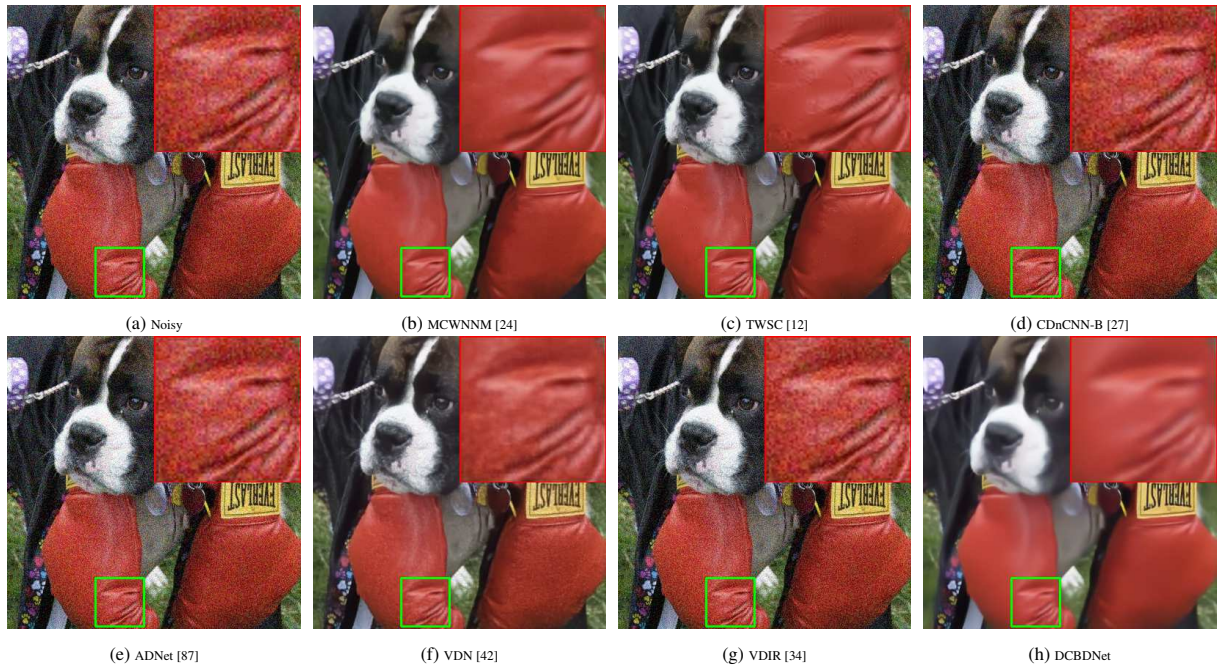


Figure 7: Visual results on the image “Dog” from RNI15 dataset.

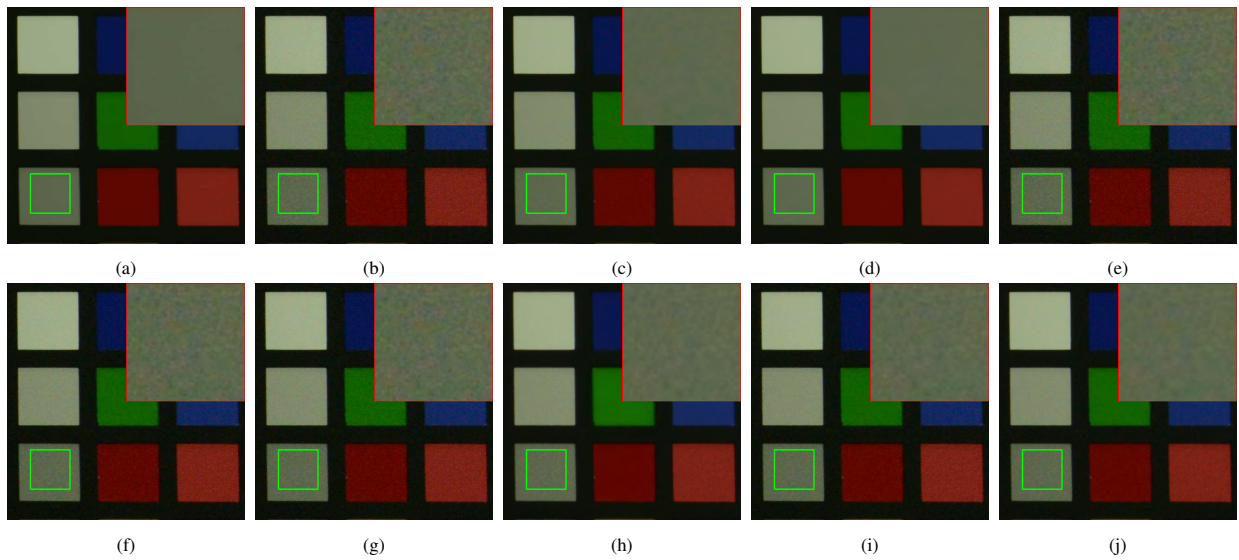


Figure 8: Denoising results on the image “Vinegar” from Nam dataset. (a) Ground-truth image / (PSNR(dB)/SSIM), (b) Noisy image / (34.93/0.841), (c) MCWNNM / (39.51/0.964), (d) TWSC / (41.05/0.983), (e) CDnCNN-B / (35.41/0.856), (f) BUFD / (35.88/0.868), (g) ADNet / (35.07/0.844), (I) VDN / (37.53/0.967), (i) VDIR / (36.88/0.909), (j) DCBDNet / (38.59/0.954).

these methods. It can be discovered that with a smaller number of parameters, our DCBDNet still can outperform some models with more network parameters in some noise levels, such as the BUIFD, DudeNet, RIDNet, CBDNet, BRDNet, and AirNet. In terms of FLOPs, we also tested the different models on two images of the same size with different channel numbers (grayscale and color). It can be found that the FLOPs of our DCBDNet are lower than most of the state-of-the-art methods, nevertheless our DCBDNet can still obtain competitive denoising performance. The experimental results also demonstrate that our DCBDNet can achieve a desirable balance between model complexity and denoising performance.

Table 10: Running time (in seconds) of the evaluated denoising methods on three grayscale and color images with different sizes.

Methods	Device	$256 \times 256$		$512 \times 512$		$1024 \times 1024$	
		Gray	Color	Gray	Color	Gray	Color
BM3D [6]	CPU	0.458	0.593	2.354	3.771	9.782	12.818
WNNM [23]	CPU	63.867	-	277.003	-	1150.842	-
MCWNNM [24]	CPU	-	62.777	-	277.623	-	1120.112
TWSC [12]	CPU	12.314	34.41	53.155	140.964	221.507	608.492
DnCNN-B [27]	GPU	0.032	0.032	0.037	0.037	0.057	0.057
BUIFD [33]	GPU	0.035	0.037	0.050	0.053	0.112	0.123
IRCNN [42]	GPU	0.030	0.030	0.030	0.030	0.030	0.030
FFDNet [30]	GPU	0.031	0.030	0.031	0.030	0.032	0.030
ADNet [87]	GPU	0.031	0.033	0.035	0.045	0.051	0.093
VDN [34]	GPU	0.144	0.162	0.607	0.597	2.367	2.376
VDIR [49]	GPU	-	0.385	-	1.622	-	6.690
DeamNet [46]	GPU	0.054	-	0.121	-	0.392	-
AirNet [47]	GPU	-	0.143	-	0.498	-	2.501
DRUNet [31]	GPU	0.068	0.068	0.106	0.107	0.276	0.280
DCBDNet	GPU	0.050	0.051	0.078	0.081	0.183	0.187

Table 11: The number of model parameters (in K) and the FLOPs (in G) for grayscale and color image denoising of different models.

Methods	Parameters		FLOPs	
	Gray	Color	$256 \times 256 \times 1$	$256 \times 256 \times 3$
DnCNN-B [27]	666	668	21.93	22.12
BUIFD [33]	1186	1196	35.31	35.65
IRCNN [42]	186	188	6.08	6.15
FFDNet [30]	485	852	3.97	3.14
CBDNet [32]	-	4365	-	20.14
RIDNet [56]	1497	1499	48.90	48.98
VDN [34]	7810	7817	24.47	24.70
VDIR [49]	-	2227	-	-
BRDNet [36]	1113	1117	36.48	36.63
ADNet [87]	519	521	17.08	17.15
DudeNet [37]	1077	1079	35.35	35.43
DeamNet [46]	2226	-	72.85	-
AirNet [47]	-	8930	-	150.64
DRUNet [31]	32639	33641	71.71	71.79
DCBDNet	1004	1013	24.38	24.68

## 5. Conclusion

In this paper, we propose a novel dual convolutional blind denoising network with skip connection (DCBDNet). The proposed DCBDNet contains a noise estimation network and a dual convolutional neural network (CNN) with two sub-networks. The proposed denoising model incorporates a noise estimation network to estimate the noise level map to enhance its flexibility, which makes the DCBDNet can achieve blind denoising. The dual CNN not only expands the network width to enhance the learning ability of the DCBDNet model, but also can capture the complementary image features for improving denoising performance. In addition, the u-shaped structure and dilated convolution are utilized in two sub-networks respectively to enlarge the receptive fields. Skip connections are adopted in both sub-networks for image feature superposing, and for avoiding the gradient vanishing or exploding. Experimental results illustrate that our proposed DCBDNet can achieve competitive denoising performance both quantitatively and qualitatively compared to state-of-the-art denoising methods. Moreover, the proposed DCBDNet has a shorter running time, fewer FLOPs, and fewer model parameters compared to many other denoising methods. Therefore our proposed DCBDNet can provide an option for practical image denoising. In the future, we aim to further investigate the feature learning ability of the model, especially for the images containing rich repetitive textures.

## 6. Acknowledgements

The work is funded by the Natural Science Foundation of China No. 61863037, No. 41971392, and the Applied Basic Research Foundation of Yunnan Province under grant No. 202001AT070077.

## References

- [1] P. Chatterjee, P. Milanfar, Is denoising dead?, *IEEE Transactions on Image Processing* 19 (4) (2010) 895–911.
- [2] A. Buades, B. Coll, J. Morel, A non-local algorithm for image denoising, in: *IEEE Conference on Computer Vision and Pattern Recognition*, 2005, pp. 60–65.
- [3] H. Li, C. Y. Suen, A novel non-local means image denoising method based on grey theory, *Pattern Recognit.* 49 (2016) 237–248.
- [4] D. Ju-Long, Control problems of grey systems, *Systems & Control Letters* 1 (5) (1982) 288–294.
- [5] E. Luo, S. H. Chan, T. Q. Nguyen, Adaptive image denoising by targeted databases, *IEEE Trans. Image Process.* 24 (7) (2015) 2167–2181.
- [6] K. Dabov, A. Foi, V. Katkovnik, K. O. Egiazarian, Image denoising by sparse 3-d transform-domain collaborative filtering, *IEEE Trans. Image Process.* 16 (8) (2007) 2080–2095.
- [7] J. Mairal, F. R. Bach, J. Ponce, G. Sapiro, A. Zisserman, Non-local sparse models for image restoration, in: *IEEE International Conference on Computer Vision*, 2009, pp. 2272–2279.
- [8] A. Buades, B. Coll, J. M. Morel, Nonlocal image and movie denoising, *International Journal of Computer Vision* 76 (2) (2008) 123–139.
- [9] J. Xu, L. Zhang, W. Zuo, D. Zhang, X. Feng, Patch group based nonlocal self-similarity prior learning for image denoising, in: *IEEE International Conference on Computer Vision*, 2015, pp. 244–252.
- [10] M. Elad, M. Aharon, Image denoising via sparse and redundant representations over learned dictionaries, *IEEE Trans. Image Process.* 15 (12) (2006) 3736–3745.
- [11] Z. Zha, X. Liu, X. Huang, H. Shi, Y. Xu, Q. Wang, L. Tang, X. Zhang, Analyzing the group sparsity based on the rank minimization methods, in: *IEEE International Conference on Multimedia and Expo*, 2017, pp. 883–888.
- [12] J. Xu, L. Zhang, D. Zhang, A trilateral weighted sparse coding scheme for real-world image denoising, in: *European Conference on Computer Vision*, Vol. 11212, 2018, pp. 21–38.
- [13] S. J. Osher, M. Burger, D. Goldfarb, J. Xu, W. Yin, An iterative regularization method for total variation-based image restoration, *Multiscale Model. Simul.* 4 (2) (2005) 460–489.
- [14] Y. Weiss, W. T. Freeman, What makes a good model of natural images?, in: *IEEE Conference on Computer Vision and Pattern Recognition*, 2007, pp. 1–8.
- [15] A. Beck, M. Teboulle, Fast gradient-based algorithms for constrained total variation image denoising and deblurring problems, *IEEE Trans. Image Process.* 18 (11) (2009) 2419–2434.
- [16] W. Zuo, L. Zhang, C. Song, D. Zhang, H. Gao, Gradient histogram estimation and preservation for texture enhanced image denoising, *IEEE Trans. Image Process.* 23 (6) (2014) 2459–2472.
- [17] X. Lan, S. Roth, D. P. Huttenlocher, M. J. Black, Efficient belief propagation with learned higher-order markov random fields, in: *European Conference on Computer Vision*, Vol. 3952, 2006, pp. 269–282.
- [18] S. Roth, M. J. Black, Fields of experts, *Int. J. Comput. Vis.* 82 (2) (2009) 205–229.
- [19] A. Barbu, Learning real-time MRF inference for image denoising, in: *IEEE Conference on Computer Vision and Pattern Recognition*, 2009, pp. 1574–1581.
- [20] A. Barbu, Training an active random field for real-time image denoising, *IEEE Trans. Image Process.* 18 (11) (2009) 2451–2462.
- [21] A. Chambolle, An algorithm for total variation minimization and applications, *J. Math. Imaging Vis.* 20 (1-2) (2004) 89–97.
- [22] C. Louchet, L. Moisan, Total variation denoising using iterated conditional expectation, in: *European Signal Processing Conference*, 2014, pp. 1592–1596.

- [23] S. Gu, L. Zhang, W. Zuo, X. Feng, Weighted nuclear norm minimization with application to image denoising, in: IEEE Conference on Computer Vision and Pattern Recognition, 2014, pp. 2862–2869.
- [24] J. Xu, L. Zhang, D. Zhang, X. Feng, Multi-channel weighted nuclear norm minimization for real color image denoising, in: IEEE International Conference on Computer Vision, 2017, pp. 1105–1113.
- [25] U. Schmidt, S. Roth, Shrinkage fields for effective image restoration, in: IEEE Conference on Computer Vision and Pattern Recognition, 2014, pp. 2774–2781.
- [26] Y. Chen, T. Pock, Trainable nonlinear reaction diffusion: A flexible framework for fast and effective image restoration, *IEEE Trans. Pattern Anal. Mach. Intell.* 39 (6) (2017) 1256–1272.
- [27] K. Zhang, W. Zuo, Y. Chen, D. Meng, L. Zhang, Beyond a gaussian denoiser: Residual learning of deep CNN for image denoising, *IEEE Trans. Image Process.* 26 (7) (2017) 3142–3155.
- [28] C. Tian, L. Fei, W. Zheng, Y. Xu, W. Zuo, C.-W. Lin, Deep learning on image denoising: An overview, *Neural Networks* 131 (2020) 251–275.
- [29] W. Wu, M. Chen, Y. Xiang, Y. Zhang, Y. Yang, Recent progress in image denoising: A training strategy perspective, *IET Image Processing* (2023) 1–31.
- [30] K. Zhang, W. Zuo, L. Zhang, Ffdnet: Toward a fast and flexible solution for cnn-based image denoising, *IEEE Trans. Image Process.* 27 (9) (2018) 4608–4622.
- [31] K. Zhang, Y. Li, W. Zuo, L. Zhang, L. Van Gool, R. Timofte, Plug-and-play image restoration with deep denoiser prior, *IEEE Transactions on Pattern Analysis and Machine Intelligence*.
- [32] S. Guo, Z. Yan, K. Zhang, W. Zuo, L. Zhang, Toward convolutional blind denoising of real photographs, in: IEEE Conference on Computer Vision and Pattern Recognition, 2019, pp. 1712–1722.
- [33] M. E. Helou, S. Süsstrunk, Blind universal bayesian image denoising with gaussian noise level learning, *IEEE Trans. Image Process.* 29 (2020) 4885–4897.
- [34] Z. Yue, H. Yong, Q. Zhao, D. Meng, L. Zhang, Variational denoising network: Toward blind noise modeling and removal, in: *Advances in Neural Information Processing Systems*, 2019, pp. 1688–1699.
- [35] J. Pan, S. Liu, D. Sun, J. Zhang, Y. Liu, J. Ren, Z. Li, J. Tang, H. Lu, Y.-W. Tai, M.-H. Yang, Learning dual convolutional neural networks for low-level vision, in: IEEE Conference on Computer Vision and Pattern Recognition, 2018, pp. 3070–3079.
- [36] C. Tian, Y. Xu, W. Zuo, Image denoising using deep CNN with batch renormalization, *Neural Networks* 121 (2020) 461–473.
- [37] C. Tian, Y. Xu, W. Zuo, B. Du, C. Lin, D. Zhang, Designing and training of a dual CNN for image denoising, *Knowl. Based Syst.* 226 (2021) 106949.
- [38] K. He, X. Zhang, S. Ren, J. Sun, Deep residual learning for image recognition, in: IEEE Conference on Computer Vision and Pattern Recognition, 2016, pp. 770–778.
- [39] G. Huang, Z. Liu, L. van der Maaten, K. Q. Weinberger, Densely connected convolutional networks, in: IEEE Conference on Computer Vision and Pattern Recognition, 2017, pp. 2261–2269.
- [40] F. Yu, V. Koltun, Multi-scale context aggregation by dilated convolutions, in: *International Conference on Learning Representations*, 2016.
- [41] O. Ronneberger, P. Fischer, T. Brox, U-net: Convolutional networks for biomedical image segmentation, in: *Medical Image Computing and Computer-Assisted Intervention*, Vol. 9351, 2015, pp. 234–241.
- [42] K. Zhang, W. Zuo, S. Gu, L. Zhang, Learning deep CNN denoiser prior for image restoration, in: IEEE Conference on Computer Vision and Pattern Recognition, 2017, pp. 2808–2817.
- [43] Y. Peng, L. Zhang, S. Liu, X. Wu, Y. Zhang, X. Wang, Dilated residual networks with symmetric skip connection for image denoising, *Neurocomputing* 345 (2019) 67–76.
- [44] J. Gurrola-Ramos, O. S. Dalmau, T. E. Alarcón, A residual dense u-net neural network for image denoising, *IEEE Access* 9 (2021) 31742–31754.
- [45] F. Jia, W. H. Wong, T. Zeng, Ddunet: Dense dense u-net with applications in image denoising, in: *International Conference on Computer Vision Workshops*, 2021, pp. 354–364.
- [46] C. Ren, X. He, C. Wang, Z. Zhao, Adaptive consistency prior based deep network for image denoising, in: IEEE Conference on Computer Vision and Pattern Recognition, 2021, pp. 8596–8606.
- [47] B. Li, X. Liu, P. Hu, Z. Wu, J. Lv, X. Peng, All-in-one image restoration for unknown corruption, in: IEEE Conference on Computer Vision and Pattern Recognition, 2022.
- [48] K. He, H. Fan, Y. Wu, S. Xie, R. Girshick, Momentum contrast for unsupervised visual representation learning, in: IEEE Conference on Computer Vision and Pattern Recognition, 2020, pp. 9726–9735.
- [49] J. W. Soh, N. I. Cho, Variational deep image restoration, *IEEE Trans. Image Process.* 31 (2022) 4363–4376.
- [50] M. Shensa, The discrete wavelet transform: wedding the a trous and mallat algorithms, *IEEE Transactions on Signal Processing* 40 (10) (1992) 2464–2482.
- [51] J. Yu, X. Yang, F. Gao, D. Tao, Deep multimodal distance metric learning using click constraints for image ranking, *IEEE Transactions on Cybernetics* 47 (12) (2017) 4014–4024.
- [52] P. Wang, P. Chen, Y. Yuan, D. Liu, Z. Huang, X. Hou, G. Cottrell, Understanding convolution for semantic segmentation, in: IEEE Winter Conference on Applications of Computer Vision, 2018, pp. 1451–1460.
- [53] X. Mao, C. Shen, Y. Yang, Image restoration using very deep convolutional encoder-decoder networks with symmetric skip connections, in: *Advances in Neural Information Processing Systems*, 2016, pp. 2802–2810.
- [54] C. Chen, Z. Xiong, X. Tian, F. Wu, Deep boosting for image denoising, in: *European Conference on Computer Vision*, Vol. 11215, 2018, pp. 3–19.
- [55] C. Chen, Z. Xiong, X. Tian, Z. Zha, F. Wu, Real-world image denoising with deep boosting, *IEEE Trans. Pattern Anal. Mach. Intell.* 42 (12) (2020) 3071–3087.
- [56] S. Anwar, N. Barnes, Real image denoising with feature attention, in: *International Conference on Computer Vision*, 2019, pp. 3155–3164.
- [57] S. Anwar, C. P. Huynh, F. Porikli, Identity enhanced residual image denoising, in: IEEE Conference on Computer Vision and Pattern Recognition, 2020, pp. 2201–2210.

- [58] M. Ranzato, Y. Boureau, Y. LeCun, Sparse feature learning for deep belief networks, in: *Advances in Neural Information Processing Systems*, 2007, pp. 1185–1192.
- [59] W. Huang, Y. Xue, L. Hu, H. Liuli, S-eegnet: Electroencephalogram signal classification based on a separable convolution neural network with bilinear interpolation, *IEEE Access* 8 (2020) 131636–131646.
- [60] S. Ioffe, C. Szegedy, Batch normalization: Accelerating deep network training by reducing internal covariate shift, in: *International Conference on Machine Learning*, Vol. 37, 2015, pp. 448–456.
- [61] A. Krizhevsky, I. Sutskever, G. E. Hinton, Imagenet classification with deep convolutional neural networks, in: *Advances in Neural Information Processing Systems*, 2012, pp. 1106–1114.
- [62] W. Malfliet, W. Hereman, The tanh method: I. exact solutions of nonlinear evolution and wave equations, *Physica Scripta* 54 (6) (1996) 563.
- [63] D. Mishkin, J. Matas, All you need is a good init, in: *International Conference on Learning Representations*, 2016.
- [64] D. Xie, J. Xiong, S. Pu, All you need is beyond a good init: Exploring better solution for training extremely deep convolutional neural networks with orthonormality and modulation, in: *IEEE Conference on Computer Vision and Pattern Recognition*, 2017, pp. 5075–5084.
- [65] K. Jia, D. Tao, S. Gao, X. Xu, Improving training of deep neural networks via singular value bounding, in: *IEEE Conference on Computer Vision and Pattern Recognition*, 2017, pp. 3994–4002.
- [66] C. Szegedy, W. Liu, Y. Jia, P. Sermanet, S. Reed, D. Anguelov, D. Erhan, V. Vanhoucke, A. Rabinovich, Going deeper with convolutions, in: *IEEE Conference on Computer Vision and Pattern Recognition*, 2015, pp. 1–9.
- [67] Y. Zhang, Y. Tian, Y. Kong, B. Zhong, Y. Fu, Residual dense network for image super-resolution, in: *IEEE Conference on Computer Vision and Pattern Recognition*, 2018, pp. 2472–2481.
- [68] W. Lai, J. Huang, N. Ahuja, M. Yang, Deep laplacian pyramid networks for fast and accurate super-resolution, *IEEE Conference on Computer Vision and Pattern Recognition* (2017) 5835–5843.
- [69] K. Jiang, Z. Wang, P. Yi, C. Chen, B. Huang, Y. Luo, J. Ma, J. Jiang, Multi-scale progressive fusion network for single image deraining, *IEEE Conference on Computer Vision and Pattern Recognition* (2020) 8343–8352.
- [70] B. Kamgar-Parsi, A. Rosenfeld, Optimally isotropic laplacian operator, *IEEE Trans. Image Process.* 8 (10) (1999) 1467–1472.
- [71] E. Agustsson, R. Timofte, NTIRE 2017 challenge on single image super-resolution: Dataset and study, in: *IEEE Conference on Computer Vision and Pattern Recognition Workshops*, 2017, pp. 1122–1131.
- [72] S. Roth, M. J. Black, Fields of experts: A framework for learning image priors, in: *IEEE Computer Society Conference on Computer Vision and Pattern*, 2005, pp. 860–867.
- [73] R. Franzen, Kodak lossless true color image suite, <http://r0k.us/graphics/kodak/> (1999).
- [74] L. Zhang, X. Wu, A. Buades, X. Li, Color demosaicking by local directional interpolation and nonlocal adaptive thresholding, *Journal of Electronic Imaging* 20 (2) (2011) 1–17.
- [75] A. Abdelhamed, S. Lin, M. S. Brown, A high-quality denoising dataset for smartphone cameras, *IEEE Conference on Computer Vision and Pattern Recognition* (2018) 1692–1700.
- [76] J. Anaya, A. Barbu, RENOIR - A dataset for real low-light image noise reduction, *J. Vis. Commun. Image Represent.* 51 (2018) 144–154.
- [77] T. Plotz, S. Roth, Benchmarking denoising algorithms with real photographs, *IEEE Conference on Computer Vision and Pattern Recognition*.
- [78] M. Lebrun, M. Colom, J. Morel, The noise clinic: a blind image denoising algorithm, *Image Process On Line* 5 (2015) 1–54.
- [79] S. Nam, Y. Hwang, Y. Matsushita, S. J. Kim, A holistic approach to cross-channel image noise modeling and its application to image denoising, in: *IEEE Conference on Computer Vision and Pattern Recognition*, 2016, pp. 1683–1691.
- [80] M. Bevilacqua, A. Roumy, C. Guillemot, M. Alberi-Morel, Low-complexity single-image super-resolution based on nonnegative neighbor embedding, in: *British Machine Vision Conference*, 2012, pp. 1–10.
- [81] D. P. Kingma, J. Ba, Adam: A method for stochastic optimization, in: *International Conference on Learning Representations*, 2015.
- [82] I. Loshchilov, F. Hutter, SGDR: stochastic gradient descent with warm restarts, *International Conference on Learning Representations*.
- [83] Z. Wang, A. C. Bovik, H. R. Sheikh, E. P. Simoncelli, Image quality assessment: from error visibility to structural similarity, *IEEE Trans. Image Process.* 13 (4) (2004) 600–612.
- [84] L. Zhang, L. Zhang, X. Mou, D. Zhang, FSIM: A feature similarity index for image quality assessment, *IEEE Trans. Image Process.* 20 (8) (2011) 2378–2386.
- [85] R. Zhang, P. Isola, A. A. Efros, E. Shechtman, O. Wang, The unreasonable effectiveness of deep features as a perceptual metric, in: *IEEE Conference on Computer Vision and Pattern Recognition*, 2018, pp. 586–595.
- [86] T. Salimans, I. J. Goodfellow, W. Zaremba, V. Cheung, A. Radford, X. Chen, Improved techniques for training gans, in: *Advances in Neural Information Processing Systems*, 2016, pp. 2226–2234.
- [87] C. Tian, Y. Xu, Z. Li, W. Zuo, L. Fei, H. Liu, Attention-guided CNN for image denoising, *Neural Networks* 124 (2020) 117–129.
- [88] Y. Quan, Y. Chen, Y. Shao, H. Teng, Y. Xu, H. Ji, Image denoising using complex-valued deep CNN, *Pattern Recognit.* 111 (2021) 107639.
- [89] Y. Liu, S. Anwar, L. Zheng, Q. Tian, Gradnet image denoising, in: *IEEE Conference on Computer Vision and Pattern Recognition*, 2020, pp. 2140–2149.